MONTANA STATE UNIVERSITY LIBRARY

Gel-Entrapped *Staphylococcus aureus* Bacteria as Models of Biofilm Infection Exhibit Growth in Dense Aggregates Oxygen Limitation, Antibiotic Tolerance, and Heterogeneous Gene Expression

Authors: Breana Pabst, Betsey Pitts, Ellen Lauchnor, & Philip S. Stewart

This is a postprint of an article that originally appeared in Antimicrobial Agents and Chemotherapy on August 2016. DOI:10.1128/AAC.01336-16.

Pabst B, Pitts B, Lauchnor E, Stewart PS, “Gel-Entrapped *Staphylococcus aureus* Bacteria as Models of Biofilm Infection Exhibit Growth in Dense Aggregates Oxygen Limitation, Antibiotic Tolerance, and Heterogeneous Gene Expression,” Antimicrobial Agents and Chemotherapy, 2016 September 23;60(10):6294-301.

Made available through Montana State University’s ScholarWorks
scholarworks.montana.edu

Gel-Entrapped *Staphylococcus aureus* Bacteria as Models of Biofilm Infection Exhibit Growth in Dense Aggregates, Oxygen Limitation, Antibiotic Tolerance, and Heterogeneous Gene Expression

Breana Pabst, Betsey Pitts, Ellen Lauchnor, Philip S. Stewart

An experimental model that mimicked the structure and characteristics of *in vivo* biofilm infections, such as those occurring in the lung or in dermal wounds where no biomaterial surface is present, was developed. In these infections, microbial biofilm forms as cell aggregates interspersed in a layer of mucus or host matrix material. This structure was modeled by filling glass cap-illary tubes with an agarose gel that had been seeded with *Staphylococcus aureus* bacteria and then incubating the gel biofilm in medium for up to 30 h. Confocal microscopy showed that the bacteria formed in discrete pockets distributed throughout the gel matrix. These aggregates enlarged over time and also developed a size gradient, with the clusters being larger near the nutrient-and oxygen-supplied interface and smaller at greater depths. Bacteria entrapped in gels for 24 h grew slowly (specific growth rate, 0.06 h^{-1}) and were much less susceptible to oxacillin, minocycline, or ciprofloxacin than planktonic cells. Microelectrode measurements showed that the oxygen concentration decreased with depth into the gel biofilm, falling to values less than 3% of air saturation at depths of 500 μm. An anaerobiosis-responsive green fluorescent protein reporter gene for lactate dehydroge-nase was induced in the region of the gel where the measured oxygen concentrations were low, confirming biologically relevant hypoxia. These results show that the gel biofilm model captures key features of biofilm infection in mucus or compromised tis-sue: formation of dense, distinct aggregates, reduced specific growth rates, local hypoxia, and antibiotic tolerance.

Numerous examples of persistent infections involving a biofilm etiology (1, 2) challenge the conventional conceptualization of biofilm formation in which a solid attachment surface is required. Particularly salient are infections such as those in the lungs of people with cystic fibrosis and patients with chronic wounds, osteomyelitis, or chronic rhinosinusitis that involve no polymer or metal implant. It has been assumed that biofilm at-tachment in these situations was to an epithelial or bony surface, but this assumption is called into question by mounting micro-scope observations of clinical specimens revealing a different or-ganization: small aggregates of biofilm-like microbial cells dis-persed in mucus or compromised soft tissue (3–5). In this alternative structure, microbial clusters are admixed with exten-sive host polymers and debris and also host immune cells span-ning a spectrum of viability (6). Even in infections where there is a foreign implant surface, such as those associated with prosthetic joints, direct microscopic observations suggest that significant numbers of microorganisms are organized in aggregates in the tissue adjacent to the implant rather than solely on the implant surface itself (3, 7–9).

This shifting concept of biofilm structure in vivo inspires alternative in vitro models for the investigation of biofilms in which microorganisms are embedded in hydrogels. There is a substantial history of using gel-entrapped microorganisms as model biofilms (10), particularly as a means of simulating reduced susceptibility to biocides, disinfectants, and antibiotics (11–15). Gel matrices that have been used to create artificial biofilms include alginate, agarose, agar, poloxamer, gelatin, and collagen. Microorganisms ranging from sulfate-reducing bacteria and Saccharomyces cerevi-siae baker's yeast to pathogens such as Pseudomonas aeruginosa and Staphylococcus aureus have been investigated in gel biofilm models. More recently, gel-entrapped bacterial systems have been specifically tailored to mimic aspects of biofilm formation *in vivo* (16–18). A long-standing animal model of chronic lung infection makes use of bacteria entrapped in agar beads (19).

The purpose of the work reported in this article was to provide an integrated characterization of an *in vitro* model of gel-embedded *S. aureus*. The characterization encompassed the dynamics and spatial organization of bacterial growth in the gel, the antibiotic tolerance of these microorganisms, microscale oxygen concentration gradients, and the physiological activity of the bacteria.

MATERIALS AND METHODS

Bacteria and media. S. *aureus* strain AH2547 was kindly provided by Alex Horswill. This strain was parent strain HG001 containing plasmid pCM29 (20). It was chosen for its strong constitutive expression of green fluores-cent protein (GFP), which facilitated the microscopic characterization of the biofilm structure. *S. aureus* bacteria derived from osteomyelitis isolate UAMS-1 with plasmid pEM87 contained a reporter construct in which the promoter for the lactate dehydrogenase gene was fused to a *gfp* gene (21). This strain was kindly provided by Ken Bayles. Inocula were grown

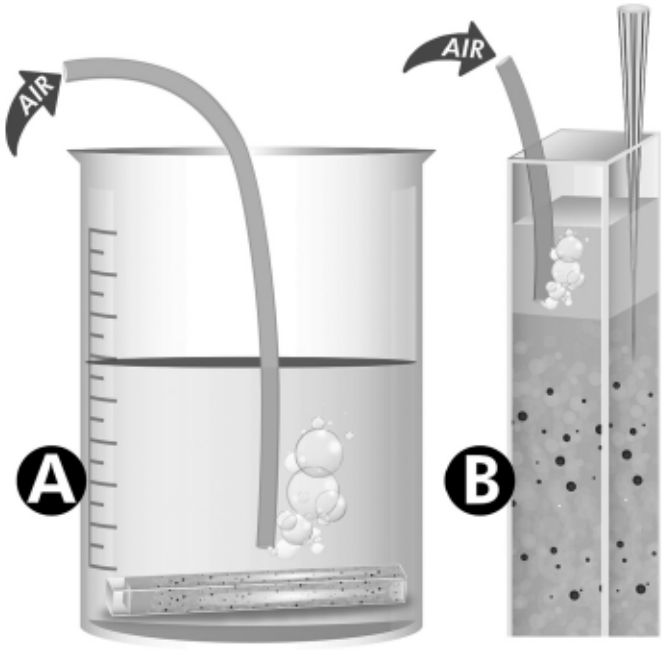


FIG 1 Experimental system. (A) Square glass capillary tubes were loaded with agarose gel seeded with *S. aureus* and then submerged in air-sparged 1/10-strength TSB. (B) After 24 h of incubation, oxygen profiles were measured by probing with an oxygen microelectrode through the open end of the capillary tube. A small volume of air-sparged medium was placed on top of the gel biofilm to maintain hydration.

overnight at 37°C with shaking in full-strength tryptic soy broth (TSB) supplemented with 10 μg ml^{-1} chloramphenicol. In other experiments, bacteria were grown in either full-strength or 1/10-strength TSB, also at 37°C.

Gel preparation. Sterile polycarbonate membranes were attached to one end of a 3-mm-square glass capillary tube, 5 cm long, using small orthodontic rubber bands in order to prevent the gel from sliding in the tube. After membrane addition, the capillaries were sterilized by UV exposure. A 1-ml aliquot of an overnight culture was centrifuged for 4 min at 6,000 rpm, the supernatant was removed, and the cells were resuspended in dilution buffer (DB). For most gel experiments, 10 μl of this inoculum was added to 10 ml DB. For antibiotic susceptibility experiments in 2-h gels, 1 ml of inoculum was added to 9 ml DB. The bacterial dilution was mixed 1:1 with a freshly autoclaved 4% agarose solution to create a final concentration of 2% agarose. The mixture of agarose and bacteria was pipetted into the open end of the capillaries and allowed to harden. The capillaries were overfilled so that the excess gel could be cut using a razor blade to create a straight edge at the open end. The capillaries were incubated at 37°C in beakers with 100 ml of 1/10-strength TSB completely covering the capillaries (Fig. 1A). Air was sparged into the medium using an aquarium pump and an air stone. The airflow rate was controlled using an adjustable clamp on the tubing. The gels were transferred to fresh TSB every 24 h.

Viable cell counts. Cell counts were done by removing the rubber band and membrane from the end of the capillary and pushing the gel out of the open end of the capillary with a sterile stick. A 3-mm cube was cut from the end of the gel using a ruler and a razor blade. The gel cube was placed in 10 ml of DB and treated with a tissue homogenizer for 1 min at 5,000 rpm to break apart the gel and disperse the bacterial cells. After homogenization, the mixture was serially diluted and plated on tryptic soy agar to enumerate the cells by colony formation. Six experiments providing cell count data at various time points were performed. Two gels were sampled at each time, and the log average for the two was taken.

Microscopy and image analysis. A Leica TCS SP5 confocal scanning laser microscope was used for imaging bacterium-containing gels. Samples were prepared by removing the membrane and rubber band from the end of the capillaries and pushing the gel slightly out of the open end using a sterile stick. Images were taken from the open end with the gel slightly outside the capillary tube so that the glass did not interfere. Imaging was done with gels in a petri dish submerged in 1/10-strength TSB. A 10× (numerical aperture [NA], 0.3) water-immersible objective was used. GFP fluorescence was excited with a 488-nm laser at 30% power, and emission was collected at wavelengths of between 500 and 600 nm. Stacks of images 200 μm thick were taken at the open end of the gel at 1-μm intervals. Three positions along the open end of the gel were imaged. MetaMorph image analysis software (Molecular Devices, Sunnyvale, CA) was used to combine the stacks of images into maximum image projections. Thresholds were applied to these images to find the percentage of the area that was occupied by bacterial cells. This was repeated for six independent experiments. The integrated morphometry analysis within MetaMorph was used to find the equivalent radii of individual bacterial aggregates and their positions in the gel. Clusters with a radius smaller than 2 μm were not included in the analysis. Data from six different experiments were fit with a second-order polynomial to describe trends.

Antibiotic susceptibility. MICs were determined using a 96-well plate in accordance with standards established by the Clinical and Laboratory Standards Institute. Antibiotics were used at approximately 20 times the MIC to challenge the bacteria. Killing of planktonic bacteria was measured by diluting an overnight culture 1:1,000 in TSB, placing the diluted cultures into two identical flasks, growing the bacteria for 3 h with shaking at 160 rpm, and then adding antibiotic, either oxacillin (20 μg ml^{-1}), minocycline (50 μg ml^{-1}), or ciprofloxacin (25 μg ml^{-1}), to both flasks. After 24 h of antibiotic treatment, a 1-ml sample from each flask was centrifuged for 4 min at 6,000 rpm, the supernatant was removed, and the cells were resuspended in DB. The samples were serially diluted and plated on tryptic soy agar to measure the number of CFU per milliliter. The log reduction in bacterial counts was calculated by comparison to the viable cell count before the addition of antibiotic. Two samples, each from a separate flask, were taken at each time, and the log average for the two was used.

Killing of bacteria in the gel system was measured by adding antibiotic at the previously specified concentrations to the medium incubating 2- or 24-h-old gels and then treating the bacteria for 24 h. The gel biofilm was still in the capillary tube, and the antibiotic was delivered into the gel by diffusion from the end of the gel in contact with the antibiotic-containing medium. Plate counts were done before and after treatment to calculate the log reduction in viable cell numbers. For the 2-h gels, samples were homogenized in 5 ml of buffer, whereas 24-h gels were homogenized in 10 ml of buffer. Duplicate gels were sampled at each time, and the log average for the two was used. Three trials were done for each antibiotic in both the planktonic and gel experiments.

Oxygen concentration profiles. Oxygen concentration profiles in the gel biofilm model were measured with a Clark-type oxygen microelectrode (Fig. 1B) with a sensor tip with a 10-μm diameter (Unisense A/S, Aarhus, Denmark). The microelectrode was connected to a millivolt meter, and data were logged onto a laptop computer with Sensor Trace Pro software (Unisense). A motor-controlled micromanipulator (model MM33; Unisense) was used to move the oxygen electrode in 25-μm intervals during profile measurements. Two-point calibrations were performed using air-saturated medium and anoxic medium (sparged with nitrogen gas).

For these experiments, the capillaries were not completely filled with gel so that some space was left at the end with the membrane. After the gels had grown for 24 h, they were positioned vertically with the membrane end facing down. The gel was allowed to slide down into the capillary, and the space at the top was filled with 1/10-strength TSB. Air was blown over the surface of this medium reservoir with an aquarium pump connected to a glass pipette. The medium layer on top of the gel was refilled period-

ically to prevent the system from drying out. Measurements were taken by probing into the gel at five different locations. The experiment was duplicated.

Planktonic *ldh* reporter gene experiments. A shake flask culture of the reporter strain was grown overnight in TSB with 10 μg ml^{-1} chloramphenicol. A 1-ml sample was centrifuged, the supernatant was removed, and the cells were resuspended in DB. The cells were subcultured 1:1,000 in fresh TSB into two flasks. Both flasks were grown aerobically for 4 h in an incubator with shaking at 160 rpm and 37°C. After 4 h of growth, one of the cultures was moved into a static incubator to grow hypoxically, and the other was kept aerobic on the shaker. Images of samples from both flasks were taken at 4 h (just before one flask was moved to a static incubator), 7 h, and 24 h of growth. Samples were centrifuged and resuspended in buffer, and a 10-μl volume was placed on a microscope slide with a coverslip. Imaging was done on an inverted Leica TCS SP5 confocal microscope with a 63× (NA, 1.2) water immersion objective. GFP fluorescence was excited with a 488-nm laser at 55% power, and emission was collected at wavelengths of between 500 and 654 nm. Three different fields of view were imaged for each sample. Images were analyzed using MetaMorph image analysis software. A square region 600 pixels by 600 pixels was created in the center of the transmission image. The cells within that region were identified by doing a threshold and then creating regions around the objects. The regions were transferred to the fluorescence image, and the average intensity of the cell region was measured. Three trials were done for this experiment.

Gel biofilm *ldh* reporter gene experiments. Gel biofilms were prepared with a shake flask culture of the reporter strain as the inoculum. The gels were grown as described above, except that chloramphenicol (10 μg ml^{-1}) was added to the medium covering the capillaries. Gels were stained with propidium iodide (PI) for 45 min at a concentration of 6 μl ml^{-1} prior to imaging. Images were taken at 5, 6, 7, and 8 h of growth on a Leica TCS SP5 confocal scanning laser microscope as described above. GFP fluorescence was excited with a 488-nm laser at 55% power, and emission was collected at wavelengths of between 500 and 542 nm. PI fluorescence was excited with a 561-nm laser at 33% power, and emission was collected at wavelengths of between 573 and 650 nm. GFP fluorescent images were collected using two line averages per frame.

In MetaMorph image analysis software, a threshold was done on the red PI image to identify the cell clusters. Regions were created around the threshold area to select for the clusters. Regions were transferred to the green GFP image, and the average intensity of the clusters and their depth in the gel were measured. Three trials of this experiment were done. For each trial, the peak intensity, peak depth, and depth of no discernible expression were measured. The peak intensity was found from a third-order polynomial fit to the raw data. The peak depth and the depth of no discernible expression were measured from graphs of the raw data.

RESULTS

Bacterial growth in agarose gels. *S. aureus* inoculated into 2% agarose gels grew within the gel matrix (Fig. 2). The growth curve exhibited characteristic exponential and stationary growth phases. The specific growth rate estimated from the exponential-phase portion of the data (0 to 10 h) was 0.73 ± 0.04 h^{-1}. This value was similar to the growth rate measured in six replicate planktonic cultures of 0.71 ± 0.11 h^{-1}. Growth slowed as the system matured. For the stationary-phase portion of the data from 15 to 30 h, the estimated specific growth rate was 0.06 ± 0.02 h^{-1}.

Confocal microscopy showed that the bacteria grew in dense, discrete aggregates within the agarose gel (Fig. 3). Each aggregate appeared to arise from an individual inoculated cell or a clump of a few cells. All aggregates enlarged with time, but their size increased unevenly. At later times (15, 24, and 30 h), the clusters adjacent to the open end of the capillary and therefore closest to the nutrient and oxygen source were larger than the clusters more deeply embedded in the gel.

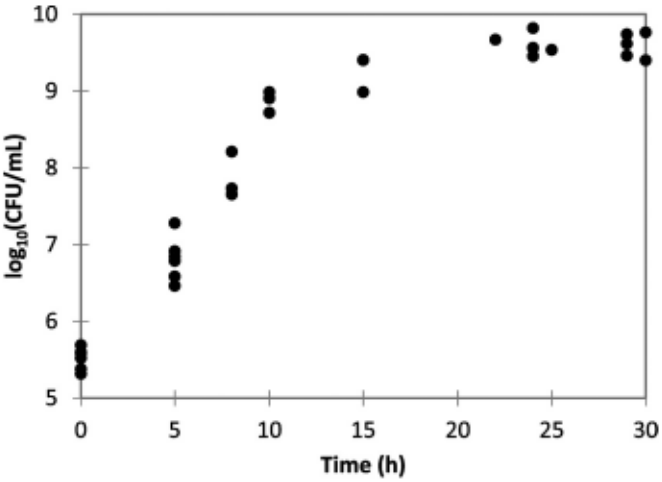


FIG 2 Growth curve for *S. aureus* AH2547 in the gel biofilm model system determined by viable plate counts. Data points show combined results from six independent experiments.

Quantitative image analysis of the area of green fluorescence in images like those in Fig. 3 recapitulated the shape of the growth curve determined from cell counts (Fig. 4). For the data obtained from 15 to 30 h, the estimated specific growth rate was 0.02 ± 0.01 h^{-1}. The size of the aggregates and their distribution with depth were measured (Fig. 5). These summary data show the development of a size gradient of aggregates with time. At time zero, the clusters were small and uniform in size. At 5 h, the clusters were slightly larger but still uniformly sized. By 8 h of growth, the aggregates were larger near the gel-nutrient interface than in the gel interior. At 30 h, aggregates as large as 50 μm in diameter were visible near the gel-nutrient interface, whereas the mean diameter of aggregates at a depth of 1.5 mm in the same gels was approximately 15 μm.

Antibiotic tolerance of bacteria in agarose gel biofilms. Bacteria entrapped in agarose gels were less susceptible to killing by all three antibiotics tested in comparison to the killing measured with planktonic cultures (Fig. 6). MICs were determined to be 0.78 μg ml^{-1}, 2.4 μg ml^{-1}, and 1.1 μg ml^{-1} for oxacillin, minocycline, and ciprofloxacin, respectively. Antibiotic challenges were performed at approximately 20× the respective MIC. Ciprofloxacin was the most effective agent but still achieved only a 1.25-log reduction in viable cell numbers in a 24-h treatment of mature (24-h-old) gel biofilms. Oxacillin and minocycline were less effective against 24-h-old biofilms, with mean log reductions of 0.48 and 0.31, respectively. Young (2-h-old) biofilms exhibited susceptibilities intermediate between those of planktonic and 24-h-old biofilm gels. Paired *t* tests between the planktonic culture, 2-h-old gel biofilm, and 24-h-old gel biofilm data sets were performed. For the comparisons of the planktonic culture and 24-h-old gel biofilm data, *P* values were 0.016 for oxacillin, 0.023 for minocycline, and 0.002 for ciprofloxacin. These values demonstrate that bacteria within 24-h-old gel biofilms were statistically significantly less susceptible to all three antibiotics than were planktonic cells. For the comparison of killing in 24-h-old gel biofilms and 2-h-old gel biofilms, *P* values were 0.004, 0.064, and 0.063 for oxacillin, mi-

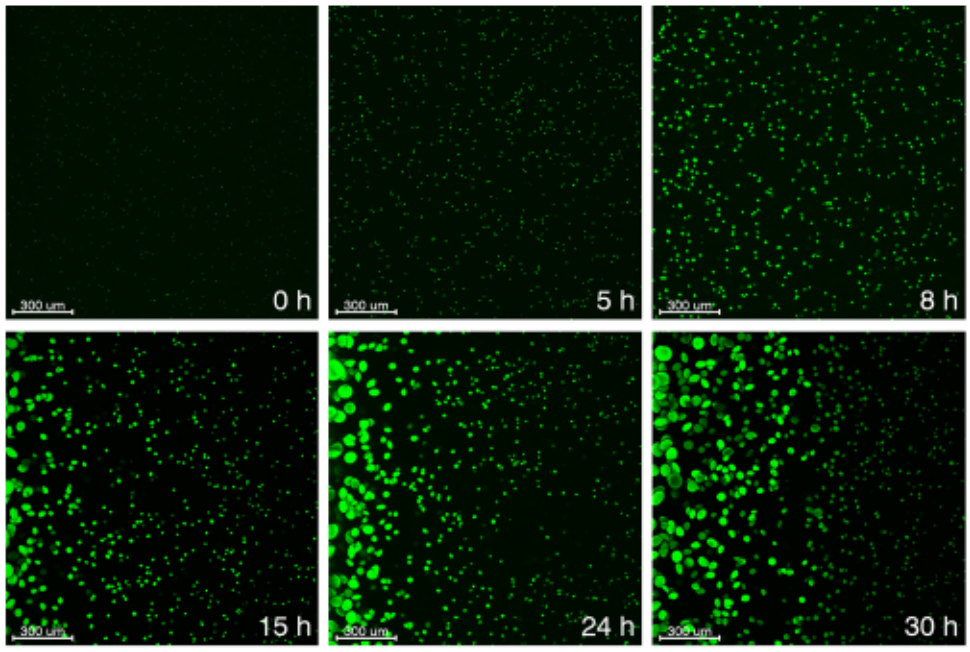


FIG 3 Representative confocal microscopy images of *S. aureus* AH2547 in the gel biofilm model at various times. The left edge of each image corresponds to the boundary of the gel directly exposed to nutrients and oxygen.

nocycline, and ciprofloxacin, respectively. In the comparison of the killing of cells in planktonic cultures with that in 2-h-old gel biofilms, *P* values were 0.099, 0.056, and 0.105 for oxacillin, minocycline, and ciprofloxacin, respectively.

Thus, for minocycline and ciprofloxacin it cannot be said that the differences between the 2-h gel biofilm data sets with either the planktonic cultures or the 24-h gel biofilm data sets were not due to random chance with a significance threshold of 0.05. The detection limit was reached in all three trials of ciprofloxacin in 2-h gels and one trial of oxacillin in 2-h gels. No growth was visible after antibiotic treatment in those experiments.

Oxygen concentration profiles in agarose gel biofilms. Oxygen profiles measured using a microelectrode revealed an oxygen concentration gradient in 24-h-old gel biofilms (Fig. 7). The oxygen concentration decreased with depth into the gel, and the gel became anoxic at approximately 500 μm into the gel.

Spatiotemporal expression of the *ldh* gene in agarose gel biofilms. Expression of the lactate dehydrogenase gene, *ldh*, has been reported to be modulated by oxygen tension in the strain of *S. aureus* used in this study(21). To confirm this relationship, we measured the average cellular fluorescence of the *ldh*::*gfp* reporter strain in parallel planktonic cultures, one of which was shaken and one of which was kept static (Fig. 8). Both cultures grew as indicated in Fig. 8 by determination of an increase in the optical den-

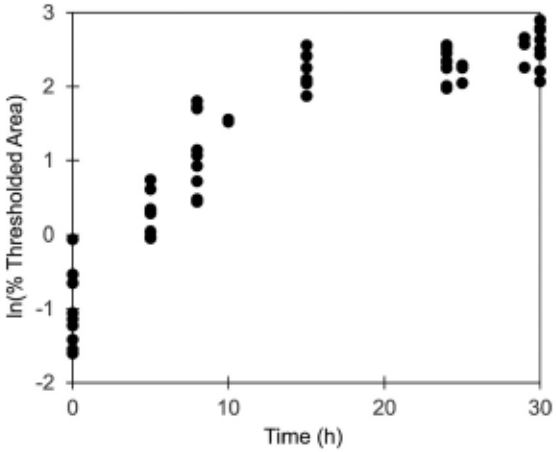


FIG 4 Growth curve for *S. aureus* AH2547 in the gel biofilm model system determined by image analysis of confocal images like those shown in Fig. 3. The area occupied by cells was determined on the basis of the green fluorescence. Data points show combined results from six independent experiments, with three images being analyzed at each sampling time.

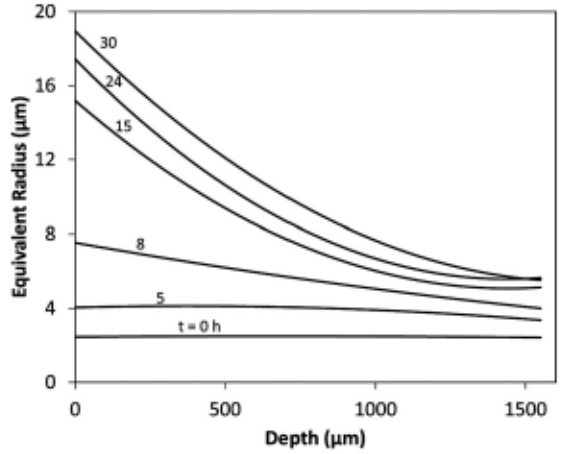


FIG 5 Size of bacterial clusters versus their depth in the gel biofilm model system, based on analysis of images like those in Fig. 3. The data for each time point were fitted with a second-order polynomial. Each of the fitted curves was derived from between 1,026 and 6,796 individual data points.

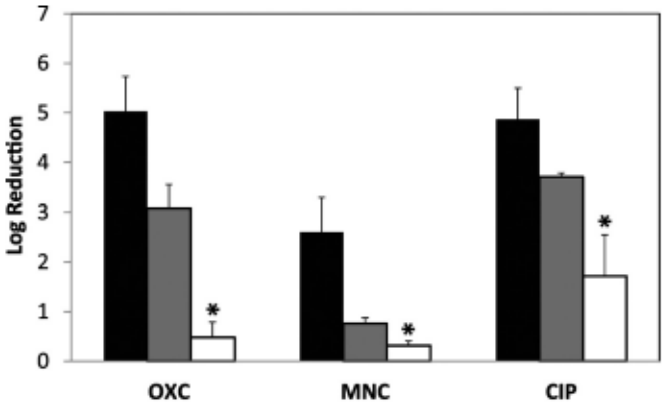


FIG 6 Comparison of killing in planktonic culture (black bars), 2-h-old gel biofilms (gray bars), and 24-h-old gel biofilms (white bars) of *S. aureus* AH2547 by three antibiotics. OXC, oxacillin; MNC, minocycline; CIP, ciprofloxacin. *, statistical significance ($P < 0.05$) for comparisons between planktonic and gel biofilm conditions.

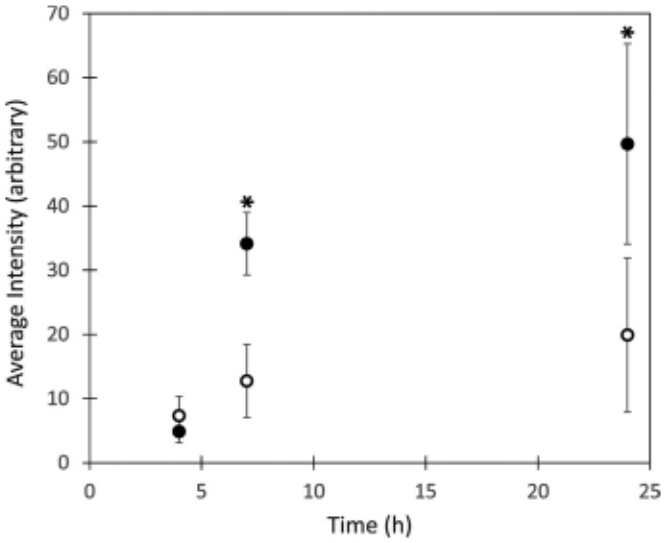


FIG 8 Average cell intensity for a shake flask culture (open circles) and a static culture (closed circles) from confocal images of planktonic cells of strain UAMS-1/pEM87 containing the *ldh*::*gfp* reporter. Both flasks were grown on the shaker for 4 h, and then one was moved to a static incubator. *, statistical significance ($P < 0.001$) for comparisons between the two culture conditions.

sity. Cells in the aerated culture developed less fluorescence than those in the static culture. A paired *t* test showed that the mean cellular fluorescence from the two cultures was statistically significantly different at both the 7-h ($P = 2 \times 10^{-6}$) and 24-h ($P = 9 \times 10^{-7}$) time points. Microscope images (not shown) of bacteria taken from planktonic cultures of the reporter strain grown aerobically and hypoxically visually confirmed that *ldh* expression was higher under conditions of less oxygen.

Confocal microscopy images of the *ldh*::*gfp* reporter strain grown in agarose gels revealed a distinct spatiotemporal pattern of fluorescence development (Fig. 9). At an early time point (Fig. 9A, 5 h), there was little detectable fluorescence. Weak fluorescence began to develop at 6 h in an interior stratum of the gel approximately 1 mm distal from the nutrient interface (Fig. 9A). The band of fluorescence became brighter and shifted toward the nutrient interface in time (Fig. 9C). From the image analysis summary shown in Table 1, the peak intensity increased with time and the peak location moved closer to the gel-nutrient interface. The dimension of the region adjacent to the gel-nutrient interface, where there was no discernible *ldh* expression, shrank in time.

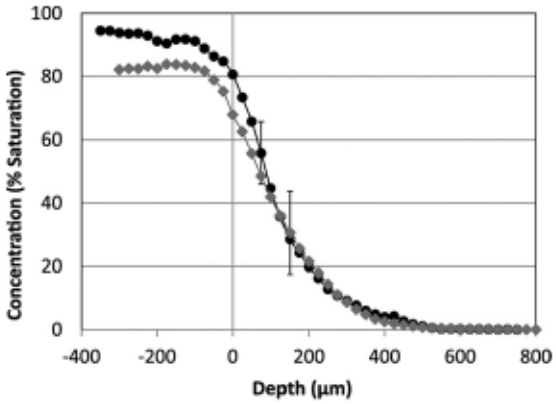


FIG 7 Oxygen concentration profiles in gel biofilms containing *S. aureus* AH2547. The data points are averages of the oxygen concentrations at five different spots in the gel. The results of two trials from two different gels are shown, and a representative error bar (standard deviation) is shown for each. Error bars on all other points were of similar magnitudes. Zero on the depth scale corresponds to the gel-nutrient medium interface.

DISCUSSION

Bacteria entrapped in a hydrogel matrix grew and generated intricate structures that captured many of the features of biofilms that form in soft tissues or mucus *in vivo*. In a system in which *S. aureus* was embedded within an agarose gel, bacteria were distributed throughout the gel in dense aggregates, approximately 5 to 50 μm in diameter, separated by regions of uncolonized gel matrix (Fig. 3). This organization, which involved no attachment substratum, neither biomaterial nor epithelium, is representative of the way in which biofilms have been described in the lungs of people with cystic fibrosis (3), in chronic wounds (5), and in periprosthetic tissue (7–9). Prior work with gel-entrapped bacteria has also reported an organization of microorganisms in dense, small clusters within the gel matrix (13, 16, 17, 22).

Bacterial growth in the gels was initially rapid, and the specific growth rate was similar to that of the planktonic cells. After a day of incubation, the specific growth rate was lowered to less than 10% of its maximum value, with estimates by two different approaches being 0.06 h^{-1} and 0.02 h^{-1}. These measurements recapitulate the observation of slow growth that has been reported in many conventional biofilm systems (23–26) and has recently been demonstrated by *ex vivo* measurements of bacterial growth rates in sputum specimens from people with cystic fibrosis (27) and in a rat model of prosthetic joint infection (28). For example, the median growth rate of *S. aureus* in the sputum of people with cystic fibrosis was 0.014 h^{-1} (27), and a typical value in the rodent joint was 0.087 h^{-1} (28). These *ex vivo* growth rates bracket the measurements in our *in vitro* gel biofilm system. The nutrient source used in this research, 1/10-strength TSB, likely provides a growth milieu richer than that found under the conditions *in vivo*. In preliminary work culturing *S. aureus* in bovine serum, for ex-

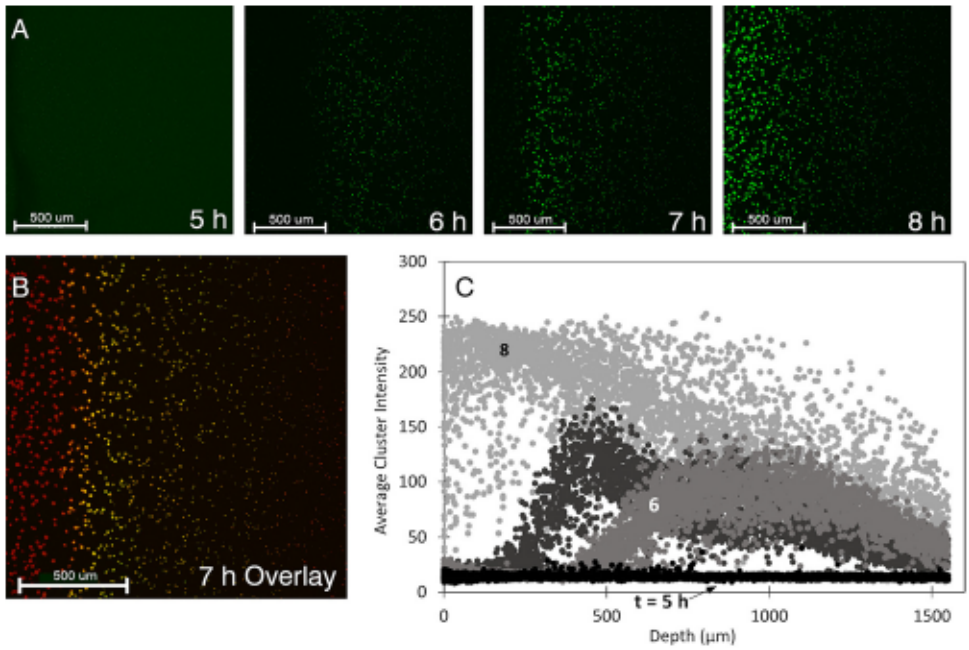


FIG 9 Analysis of *ldh*::*gfp* reporter strain UAMS-1/pEM87 in the gel biofilm system from one representative experiment. (A) Confocal images over a 3-h time period. The left edge of each image corresponds to the gel interface directly exposed to nutrients and oxygen. (B) Green fluorescence images (*ldh*::*gfp* reporter strain) at 7 h overlaid with propidium iodide (red). (C) Average cluster green fluorescence intensity versus depth in the gel from 5 to 8 h.

ample, the specific growth rate was approximately 40% of the rate measured in dilute TSB.

The *S. aureus* gel biofilm system harbors an oxygen concentration gradient (Fig. 7) and therefore represents a common feature of biofilm infections, where multiple lines of evidence point to hypoxic conditions (29–33). Hypoxia within the gel biofilm is also indicated by localized expression of the lactate dehydrogenase gene, which is expressed in the transition to anaerobiosis (Fig. 9). These signatures for local hypoxia and anaerobiosis agree with those from previous transcriptomic, proteomic, and metabolomics comparisons of planktonic and biofilm staphylococcal cells, which collectively revealed decreased aerobic energy metabolism and increased fermentative activity in biofilms (34–39). More specifically, the spatial pattern of *ldh* expression conforms to the qualitative pattern predicted for a gene whose expression is induced under conditions of diminished oxygen (40). The modeled pattern predicts maximal expression at an intermediate depth from the oxygenated interface of the biofilm. At depths closer to the oxic boundary, the oxygen concentration is too high to allow induction, and at deeper locations, the growth rate of the bacteria is too low to permit much new protein synthesis. In *S. aureus* gel biofilms formed with a hemispherical shape, complex patterns of *ldh* expression that depended on the initial density of gel inoculation were observed (41).

TABLE 1 Image analysis summary of the reporter strain UAMS-1/pEM87 in the gel system for three experiments

Expt no.	Peak intensity[a] at the following time (h):				Peak depth (μm) at the following time (h):				Depth (μm) of no expression at the following time (h):			
	5	6	7	8	5	6	7	8	5	6	7	8
1	15	95	95	195	NA[b]	900	450	0	1,515	400	250	0
2	13	14	140	95	NA	NA	500	300	1,515	1,515	170	100
3	13	16	79	105	NA	NA	550	300	1,515	1,515	300	100
Avg	13.7	41.7	104.7	131.7	NA	900	500	200	1,515	1,143.3	240	66.7

[a] Intensity units are arbitrary.
[b] NA, not applicable because no peak was present.

Though nutrient concentrations within gel biofilms were not measured, it is possible to place rough estimates on these concentrations. Because the carbonaceous substrate concentration in 1/10-strength TSB is so high (2,250 mg liter^{-1}) in comparison to the amount of oxygen available (approximately 6 mg liter^{-1} in equilibrium with air at the altitude in Bozeman, MT), oxygen is limiting (as demonstrated experimentally) and most of the carbonaceous substrates are present in excess throughout the gel biofilm. However, it is possible that concentration gradients of certain substrates that can be used in the absence of oxygen, such as glucose, which *S. aureus* can ferment, could develop. Gel biofilms were initially fabricated without nutrients in the gel matrix. The delivery of nutrients into the gel occurred by diffusion. An order-of-magnitude estimate of the depth, d, to which nutrients could diffuse in the 24-h incubation period is given by $d \approx (Dt)^{1/2}$, where the diffusion coefficient, D, of a representative substrate (here, glucose) is taken to be 7.3×10^{-6} cm^2 s^{-1} and the time (t) is 86,400 s (42). The penetration depth thus estimated is 8,000 μm. This is much greater than the experimentally observed penetration depth of oxygen of 500 μm.

Our measurements are consistent with physiological heterogeneity within the gel biofilm system. In particular, the difference in the sizes of bacterial aggregates within the gel structure (larger clusters near the nutrient- and oxygen-provisioned interface, smaller clusters deeper in the gel biofilm) presumably reflects differences in the local growth rate of the bacteria. Some earlier studies with gel-entrapped bacteria reported finding a distribution of microaggregate sizes within the gel conforming to the presumed

nutrient concentration gradient (10, 13, 22, 43). The size of a bacterial aggregate corresponds to the integrated growth over the culture period. An estimate of the relative growth rates at the surface of the gel and far from this surface can be made by comparing the volume of bacterial aggregates at these two locations. After 30 h of incubation in the agarose gel, a typical aggregate radius was 19 μm at the gel surface and 5.5 μm at a depth of 1.5 mm (Fig. 5). The ratio of these two radii equates to a 41-fold difference in aggregate volume. In other words, the average growth rate of *S. aureus* at a depth of 1.5 mm was 41 times lower than the average growth rate near the nutrient- and oxygen-fed interface. Physiological heterogeneity is a well-established characteristic of biofilms (44) that derives from reaction-diffusion interactions on metabolic substrates (42, 45).

The *S. aureus*-agarose biofilm system displayed the antibiotic tolerance that is characteristic of microbial biofilms (46). The tolerance factors (rate of killing of planktonic cells divided by the rate of killing of mature biofilm cells) for the three antibiotics used in this work were 10.5 for oxacillin, 8.4 for minocycline, and 2.8 for ciprofloxacin. These values fall within the range of tolerance factors calculated from other studies (46). These susceptibility measurements are also in accord with findings from prior work investigating gel-entrapped microorganisms (11–17, 22, 47–50). Antibiotics likely penetrate the 3-mm-deep sampling zone of the gel biofilm in the 24-h treatment period. The delivery of antibiotic into the gel by diffusion can be estimated, as was done as described above for a nutrient, from $d \approx (Dt)^{1/2}$, where the diffusion coefficient, D, of a representative antibiotic is taken to be 5×10^{-6} cm^2 s^{-1} and the time (t) is 86,400 s (42). The diffusive penetration depth calculated in this way is 6 mm.

Collectively, the results presented in this article support the emerging variation of the biofilm hypothesis that a solid attachment surface is not necessary to form communities exhibiting hypoxia, heterogeneous growth, and antibiotic tolerance (51). It appears that what is essential is that microorganisms be organized in dense aggregates within a hydrated polymer matrix whose origin may be from the microbe, the host, or synthetic material. These concepts may have relevance for understanding and treating some infections that fit the biofilm paradigm, even though no rigid substratum is present. Gel-entrapped microorganisms may provide useful models of biofilm infections that are alternatives to well-known biofilm reactor systems (52).

ACKNOWLEDGMENTS

NIH award R01GM109452 supported this work. Imaging was made possible by microscope facilities at the Center for Biofilm Engineering, which were supported by funding from the NSF-MRI Program and the M. J. Murdock Charitable Trust.

FUNDING INFORMATION

This work, including the efforts of Philip S. Stewart, was funded by HHS | National Institutes of Health (NIH) (R01GM109452). This work, including the efforts of Philip S. Stewart, was funded by National Science Foundation (NSF) (1039785).

REFERENCES

1. **Costerton JW, Stewart PS, Greenberg EP.** 1999. Bacterial biofilms: a common cause of persistent infections. Science **284**:1318–1322. http://dx.doi.org/10.1126/science.284.5418.1318.
2. **Parsek MR, Singh PK.** 2003. Bacterial biofilms: an emerging link to disease pathogenesis. Annu Rev Microbiol 57:677–701. http://dx.doi.org/10.1146/annurev.micro.57.030502.090720.
3. **Bjarnsholt T, Jensen PØ, Fiandaca MJ, Pedersen J, Hansen CR, Andersen CB, Pressler T, Givskov M, Høiby N.** 2009. *Pseudomonas aeruginosa* biofilms in the respiratory tract of cystic fibrosis patients. Pediatr Pulmonol **44**:547–558. http://dx.doi.org/10.1002/ppul.21011.
4. **Bjarnsholt T, Alhede M, Alhede M, Eickhardt-Sørensen SR, Moser C, Kühl M, Jensen PØ, Høiby N.** 2013. The *in vivo* biofilm. Trends Microbiol **21**:466–474. http://dx.doi.org/10.1016/j.tim.2013.06.002.
5. **James GA, Swogger E, Wolcott R, Pulcini ED, Secor P, Sestrich J, Costerton JW, Stewart PS.** 2008. Biofilms in chronic wounds. Wound Repair Regen **16**:37–44. http://dx.doi.org/10.1111/j.1524-475X.2007.00321.x.
6. **Stewart PS.** 2014. Biophysics of biofilm infection. Pathog Dis **70**:212–218. http://dx.doi.org/10.1111/2049-632X.12118.
7. **Stoodley P, Nistico L, Johnson S, Lasko L-A, Baratz M, Gahlot V, Ehrlich GD, Kathju S.** 2008. Direct demonstration of viable *Staphylococcus aureus* biofilms in an infected total joint arthroplasty: a case report. J Bone Joint Surg Am **90**:1751–1758. http://dx.doi.org/10.2106/JBJS.G.00838.
8. **Zaat S, Broekhuizen C, Riool M.** 2010. Host tissue as a niche for biomaterial-associated infection. Future Microbiol **5**:1149–1151. http://dx.doi.org/10.2217/fmb.10.89.
9. **Stoodley P, Conti SF, DeMeo PJ, Nistico L, Melton-Kreft R, Jonson S, Darabi A, Ehrlich GD, Costerton JW, Kathju S.** 2011. Characterization of a mixed MRSA/MRSE biofilm in an explanted total ankle arthroplasty. FEMS Immunol Med Microbiol **62**:66–74. http://dx.doi.org/10.1111/j.1574-695X.2011.00793.x.
10. **Strathmann M, Griebe T, Flemming HC.** 2000. Artificial biofilm model—a useful tool for biofilm research. Appl Microbiol Biotechnol **54**:231–237. http://dx.doi.org/10.1007/s002530000370.
11. **Whitham TS, Gilbert PD.** 1993. Evaluation of a model biofilm for the ranking of biocide performance against sulphate-reducing bacteria. J Appl Bacteriol **75**:529–535. http://dx.doi.org/10.1111/j.1365-2672.1993.tb01590.x.
12. **Tresse O, Jouenne T, Junter GA.** 1995. The role of oxygen limitation in the resistance of agar-entrapped, sessile-like *Escherichia coli* to aminoglycoside and beta-lactam antibiotics. J Antimicrob Chemother **36**:521–526. http://dx.doi.org/10.1093/jac/36.3.521.
13. **Coquet L, Junter GA, Jouenne T.** 1998. Resistance of artificial biofilms of *Pseudomonas aeruginosa* to imipenem and tobramycin. J Antimicrob Chemother **42**:755–760. http://dx.doi.org/10.1093/jac/42.6.755.
14. **Wirtanen G, Salo S, Allison DG, Mattila-Sandholm T, Gilbert P.** 1998. Performance evaluation of disinfectant formulations using poloxamer-hydrogel biofilm-constructs. J Appl Microbiol **85**:965–971. http://dx.doi.org/10.1111/j.1365-2672.1998.tb05260.x.
15. **Clutterbuck AL, Cochrane CA, Dolman J, Percival SL.** 2007. Evaluating antibiotics for use in medicine using a poloxamer biofilm model. Ann Clin Microbiol Antimicrob **6**:2. http://dx.doi.org/10.1186/1476-0711-6-2.
16. **Werthén M, Henriksson L, Jensen PØ, Sternberg C, Givskov M, Bjarnsholt T.** 2010. An *in vitro* model of bacterial infections in wounds and other soft tissues. APMIS **118**:156–164. http://dx.doi.org/10.1111/j.1600-0463.2009.02580.x.
17. **Staudinger BJ, Muller JF, Halldórsson S, Boles B, Angermeyer A, Nguyen D, Rosen H, Baldursson O, Gottfreðsson M, Guðmundsson GH, Singh PK.** 2014. Conditions associated with the cystic fibrosis defect promote chronic *Pseudomonas aeruginosa* infection. Am J Respir Crit Care Med **189**:812–824. http://dx.doi.org/10.1164/rccm.201312-2142OC.
18. **Crone S, Garde C, Bjarnsholt T, Alhede M.** 2015. A novel *in vitro* wound biofilm model used to evaluate low-frequency ultrasonic-assisted wound debridement. J Wound Care **24**:64–72. http://dx.doi.org/10.12968/jowc.2015.24.2.64.
19. **Cash HA, Woods DE, McCullogh B, Johanson WG, Jr, Bass JA.** 1979. A rat model of chronic respiratory infection with *Pseudomonas aeruginosa*. Am Rev Respir Dis **119**:453–459.
20. **Pang YY, Schwartz J, Thoendel M, Ackermann LW, Horswill AR, Nauseef WM.** 2010. agr-dependent interactions of *Staphylococcus aureus* USA300 with human polymorphonuclear neutrophils. J Innate Immun **2**:546–559. http://dx.doi.org/10.1159/000319855.
21. **Moormeier DE, Endres JL, Mann EE, Sadykov MR, Horswill A, Rice KC, Fey PD, Bayles KW.** 2013. Use of microfluidic technology to analyze gene expression during *Staphylococcus aureus* biofilm formation reveals distinct physiological niches. Appl Environ Microbiol **79**:3413–3424. http://dx.doi.org/10.1128/AEM.00395-13.
22. **Grobe KJ, Zahller J, Stewart PS.** 2002. Role of dose concentration in

biocide efficacy against *Pseudomonas aeruginosa* biofilms. J Ind Microbiol Biotechnol **29**:10–15. http://dx.doi.org/10.1038/sj.jim.7000256.

23. **Hodgson AE, Nelson SM, Brown MR, Gilbert P.** 1995. A simple in vitro model for growth control of bacterial biofilms. J Appl Bacteriol **79**:87–93. http://dx.doi.org/10.1111/j.1365-2672.1995.tb03128.x.
24. **Wentland EJ, Stewart PS, Huang C-T, McFeters GA.** 1996. Spatial variations in growth rate within *Klebsiella pneumoniae* colonies and biofilm. Biotechnol Prog **12**:316–321. http://dx.doi.org/10.1021/bp9600243.
25. **Zheng Z, Stewart PS.** 2002. Penetration of rifampin through *Staphylococcus epidermidis* biofilms. Antimicrob Agents Chemother **46**:900–903. http://dx.doi.org/10.1128/AAC.46.3.900-903.2002.
26. **Rani SA, Pitts B, Beyenal H, Veluchamy RA, Lewandowski Z, Davison WM, Buckingham-Meyer K, Stewart PS.** 2007. Spatial patterns of DNA replication, protein synthesis, and oxygen concentration within bacterial biofilms reveal diverse physiological states. J Bacteriol **189**:4223–4233. http://dx.doi.org/10.1128/JB.00107-07.
27. **Kopf SH, Sessions AL, Cowley ES, Reyes C, Van Sambeek L, Hu Y, Orphan VJ, Kato R, Newman DK.** 2016. Trace incorporation of heavy water reveals slow and heterogeneous pathogen growth rates in cystic fibrosis sputum. Proc Natl Acad Sci U S A **113**:E110–E116. http://dx.doi.org/10.1073/pnas.1512057112.
28. **Pribaz JR, Bernthal NM, Billi F, Cho JS, Ramos RI, Guo Y, Cheung AL, Francis KP, Miller LS.** 2012. Mouse model of chronic post-arthroplasty infection: noninvasive in vivo bioluminescence imaging to monitor bacterial burden for long-term study. J Orthop Res **30**:335–340. http://dx.doi.org/10.1002/jor.21519.
29. **Worlitzsch D, Tarran R, Ulrich M, Schwab U, Cekici A, Meyer KC, Birrer P, Bellon G, Berger J, Weiss T, Botzenhart K, Yankaskas JR, Randell S, Boucher RC, Döring G.** 2002. Effects of reduced mucus oxygen concentration in airway *Pseudomonas* infections of cystic fibrosis patients. J Clin Invest **109**:317–325. http://dx.doi.org/10.1172/JCI0213870.
30. **Hassett DJ, Sutton MD, Schurr MJ, Herr AB, Caldwell CC, Matu JO.** 2009. *Pseudomonas aeruginosa* hypoxic or anaerobic biofilm infections within cystic fibrosis airways. Trends Microbiol **17**:130–138. http://dx.doi.org/10.1016/j.tim.2008.12.003.
31. **Lone AG, Atci E, Renslow R, Beyenal H, Noh S, Fransson B, Abu-Lail N, Park JJ, Gang DR, Call DR.** 2015. *Staphylococcus aureus* induces hypoxia and cellular damage in porcine dermal explants. Infect Immun **83**:2531–2541. http://dx.doi.org/10.1128/IAI.03075-14.
32. **Cowley ES, Kopf SH, LaRiviere A, Ziebis W, Newman DK.** 2015. Pediatric cystic fibrosis sputum can be chemically dynamic, anoxic, and extremely reduced due to hydrogen sulfide formation. mBio **6**:e00767. http://dx.doi.org/10.1128/mBio.00767-15.
33. **James GA, Zhao GA, Usui M, Underwood RA, Nguyen H, Beyenal H, deLancey Pulcini E, Agostinho Hunt A, Bernstein HC, Fleckman P, Olerud J, Williamson KS, Franklin MJ, Stewart PS.** 2016. Microsensor and transcriptomic signatures of oxygen depletion in biofilms associated with chronic wounds. Wound Repair Regen **24**:373–383. http://dx.doi.org/10.1111/wrr.12401.
34. **Beenken KE, Dunman PM, McAleese F, Macapagal D, Murphy E, Projan SJ, Blevins JS, Smeltzer MS.** 2004. Global gene expression in *Staphylococcus aureus* biofilms. J Bacteriol **186**:4665–4684. http://dx.doi.org/10.1128/JB.186.14.4665-4684.2004.
35. **Yao Y, Sturdevant DE, Otto M.** 2005. Genomewide analysis of gene expression in *Staphylococcus epidermidis* biofilms: insights into the pathophysiology of *S. epidermidis* biofilms and the role of phenol-soluble modulins in formation of biofilms. J Infect Dis **191**:289–298. http://dx.doi.org/10.1086/426945.
36. **Resch A, Rosenstein R, Nerz C, Götz F.** 2005. Differential gene expression profiling of *Staphylococcus aureus* cultivated under biofilm and planktonic conditions. Appl Environ Microbiol **71**:2663–2676. http://dx.doi.org/10.1128/AEM.71.5.2663-2676.2005.
37. **Resch A, Leicht S, Saric M, Pásztor L, Jakob A, Götz F, Nordheim A.** 2006. Comparative proteome analysis of *Staphylococcus aureus* biofilm and planktonic cells and correlation with transcriptome profiling. Proteomics **6**:1867–1877. http://dx.doi.org/10.1002/pmic.200500531.
38. **Zhu Y, Weiss EC, Otto M, Fey PD, Smeltzer MS, Somerville GA.** 2007. *Staphylococcus aureus* biofilm metabolism and the influence of arginine on polysaccharide intercellular adhesin synthesis, biofilm formation, and pathogenesis. Infect Immun **75**:4219–4226. http://dx.doi.org/10.1128/IAI.00509-07.
39. **Ammons MC, Tripet BP, Carlson RP, Kirker KR, Gross MA, Stanisich JJ, Copié V.** 2014. Quantitative NMR metabolite profiling of methicillin-resistant and methicillin-susceptible *Staphylococcus aureus* discriminates between biofilm and planktonic phenotypes. J Proteome Res **13**:2973–2985. http://dx.doi.org/10.1021/pr500120c.
40. **Zhang T, Pabst B, Klapper I, Stewart PS.** 2013. General theory for integrated analysis of growth, gene, and protein expression in biofilms. PLoS One **8**:e83626. http://dx.doi.org/10.1371/journal.pone.0083626.
41. **Aristotelous AC, Klapper I, Grabovsky Y, Pabst B, Pitts B, Stewart PS.** 2015. Diffusive transport through a model host-biofilm system. Phys Rev E **92**:022703. http://dx.doi.org/10.1103/PhysRevE.92.022703.
42. **Stewart PS.** 2003. Diffusion in biofilms. J Bacteriol **185**:1485–1491. http://dx.doi.org/10.1128/JB.185.5.1485-1491.2003.
43. **Parascandola P, de Alteriis E.** 1996. Pattern of growth and respiratory activity of *Saccharomyces cerevisiae* (baker's yeast) cells growing entrapped in an insolubilized gelatin gel. Biotechnol Appl Biochem **23**:7–12.
44. **Stewart PS, Franklin MJ.** 2008. Physiological heterogeneity in biofilms. Nat Rev Microbiol **6**:199–210. http://dx.doi.org/10.1038/nrmicro1838.
45. **Stewart PS, Zhang T, Xu R, Pitts B, Walters MC, III, Roe F, Kikhney J, Moter A.** 2016. Reaction-diffusion theory explains hypoxia and heterogeneous growth within microbial biofilms associated with chronic infections. Biofilms Microbiomes **2**:16012. http://dx.doi.org/10.1038/npjbiofilms.2016.12.
46. **Stewart PS.** 2015. Antimicrobial tolerance in biofilms. Microbiol Spectr **3**:MB-0010-2014. http://dx.doi.org/10.1128/microbiolspec.MB-0010-2014.
47. **Cao B, Christophersen L, Thomsen K, Sønderholm M, Bjarnsholt T, Jensen PØ, Høiby N, Moser C.** 2015. Antibiotic penetration and bacterial killing in a *Pseudomonas aeruginosa* biofilm model. J Antimicrob Chemother **70**:2057–2063. http://dx.doi.org/10.1093/jac/dkv058.
48. **Chen X, Stewart PS.** 1996. Chlorine penetration into artificial biofilm is limited by a reaction-diffusion interaction. Environ Sci Technol **30**:2078–2083. http://dx.doi.org/10.1021/es9509184.
49. **Vilain S, Cosette P, Junter GA, Jouenne T.** 2002. Phosphate deprivation is associated with high resistance to latamoxef of gel-entrapped, sessile-like *Escherichia coli* cells. J Antimicrob Chemother **49**:315–320. http://dx.doi.org/10.1093/jac/49.2.315.
50. **Stewart PS, Grab L, Diemer JA.** 1998. Analysis of biocide transport limitation in an artificial biofilm system. J Appl Microbiol **85**:495–500. http://dx.doi.org/10.1046/j.1365-2672.1998.853529.x.
51. **Alhede M, Kragh KN, Qvortrup K, Allesen-Holm M, van Gennip M, Christensen LD, Jensen PØ, Nielsen AK, Parsek M, Wozniak D, Molin S, Tolker-Nielsen T, Høiby N, Givskov M, Bjarnsholt T.** 2011. Phenotypes of non-attached *Pseudomonas aeruginosa* aggregates resemble surface attached biofilm. PLoS One **6**:e27943. http://dx.doi.org/10.1371/journal.pone.0027943.
52. **Coenye T, Nelis HJ.** 2010. *In vitro* and *in vivo* model systems to study microbial biofilm formation. J Microbiol Methods **83**:89–105. http://dx.doi.org/10.1016/j.mimet.2010.08.018.